RESEARCH PAPER

# Developmental toxicity of iron oxide nanoparticles with different coatings in zebrafish larvae

E. M. N. Oliveira · G. I. Selli · A. von Schmude · C. Miguel · S. Laurent · M. R. M. Vianna · R. M. Papaléo

**Abstract** We report on the effect of different coatings (dextran, chitosan, polyethylene glycol, carboxy-silane, and silica) in the toxicity elicited by superparamagnetic iron oxide nanoparticles (SPIONs) in the developing zebrafish (*Danio rerio*). Animals were exposed to nanoparticle concentrations ranging from 0.125 to 8.0 mM of Fe during the first 5 days after fertilization. Embryotoxicity parameters (survival, hatching rate, and the incidence of anatomical malformations) and behavioral patterns (locomotion during the exploration of a new environment, thigmotaxis, and the escape response to an aversive stimulus) were evaluated. Exposed embryos hatched between 48 and 72 hpf, as expected for the species, but tendencies of either acceleration or delay were observed, depending on the nanoparticle coating. Malformations in exposed and control groups were similar, independent of the coating.

Mortality rates were also not significantly affected by exposure to most of the coated SPIONs, except for animals treated with chitosan-coated nanoparticles, which induced 100% mortality at concentrations higher than 2 mM. A similar trend was observed in the behavioral parameters, in which significant adverse effects were mostly caused by chitosan-coated nanoparticles even at low concentrations. The higher toxicity observed for chitosan-coated particles raises concern and deserves further mechanistic investigations, considering the ample use of this compound in pharmaceutical and biomedical applications.

**Keywords** Iron oxide nanoparticles · Nanotoxicity · Zebrafish (*Danio rerio*) · Embryotoxicity · Environmental and health effects

E. M. N. Oliveira · G. I. Selli · A. von Schmude ·
M. R. M. Vianna · R. M. Papaléo
Interdisciplinary Center of Nanoscience and
Micro-Nanotechnology, School of Technology, Pontifical Catholic
University of Rio Grande do Sul, Av. Ipiranga 6681, 90619-900
Porto Alegre, Brazil

E. M. N. Oliveira (✉) · C. Miguel · M. R. M. Vianna
Laboratory of Biology and Development of the Nervous System &
ZebLab, School of Health and Life Sciences, Pontifical Catholic
University of Rio Grande do Sul, Av. Ipiranga 6681, Porto
Alegre 90619-900, Brazil
e-mail: elisa.oliveira@acad.pucrs.br

S. Laurent
NMR and Molecular Imaging, University of Mons, 19 Av.
Maistriau, 7000 Mons, Belgium

## Introduction

Nanomaterials have been increasingly used in biological contexts, either when administered systemically for disease diagnosis and therapy or in implanted devices, cosmetics, and smart textiles that will be in contact with the body (Koo et al. 2005; Montet et al. 2006; Cai and Chen 2007; Som et al. 2011; Ramos et al. 2017). Nanoparticles (NPs) are also extensively used for in vivo monitoring of biological processes in pre-clinical imaging. Among the different nanoparticles, superparamagnetic iron oxides (SPIONs) are one of the most prevalent in biomedical applications (Laurent et al. 2008; Lee et al. 2015; Xue et al. 2018; Liu et al. 2019a).

SPIONs have a structure composed of a small magnetite or maghemite core (typically below 20 nm) with the surface modified by a coating layer. The coating protects the particles against the surrounding environment, minimizing aggregation. It may also provide sites for addition of chemical groups or whole molecules which will eventually give multiple functionalities to the system. SPIONs can be dispersed in different solvents, forming homogeneous suspensions (ferrofluids), which can interact with an external magnetic field and be localized at specific sites (Laurent S. et al. 2008). Therefore, SPIONS may serve as a signaling material, enhancing contrast in magnetic resonance imaging (MRI), or may act as a coupling medium to an external eletromagnetic field to induce local hyperthermia for the treatment of cancer (Josephson et al. 2002; Montet et al. 2006; Mahmoudi et al. 2011; Bañobre-López et al. 2013; Lee et al. 2015; Sharifi et al. 2015; Zhang et al. 2017; Liu et al. 2019b).

In order to evaluate the risks associated with the exposure of biological systems to nanoparticles, the effect of their coating layer must also be considered. This may be as important as other physico-chemical parameters of the particulate system, such as the particles size distribution, shape, or elemental composition (van der Merwe and Pickrell 2007; Kong et al. 2011; Liskova et al. 2017; van Pomeren et al. 2019). Here, we address this problem in an intact organism, using the developing zebrafish larvae as a model system. The zebrafish (Danio rerio) has emerged as a competitive model organism for in vivo toxicological and pharmacological studies (Hill et al. 2005; Kari et al. 2007; George et al. 2011; Liu et al. 2012). The great fecundity and rapid external development of the animal enable high-throughput analysis while the significant genomic similarity makes experimental data, in principle, translational to humans (Lieschke and Currie 2007). In addition, zebrafish is a suitable organism to investigate the risks associated to the release and accumulation of nanomaterials in the aquatic environment (Zhu et al. 2012; Lin et al. 2013; Magro et al. 2018).

In spite of the numerous works already conducted on the in vitro (Berry et al. 2004; Geiss et al. 2005; Soenen et al. 2011; Sun et al. 2013; Biyani et al. 2014) and in vivo toxicity of SPIONs (Zhu et al. 2012; De Oliveira et al. 2014; Fifi et al. 2016; de Oliveira et al. 2017; Magro et al. 2018), including in humans (Vu et al. 2004; Reimer et al. 2007; Wang 2015), there are still insufficient experimental evidence concerning the effect of different formulations in the toxicity profile of these nanoparticles. This is also true for other classes of nanoparticles (Powers et al. 2011; Osborne et al. 2013; Ahmad et al. 2015; Samaee et al. 2015; Karunaratne et al. 2017; Cambier et al. 2018; Magro et al. 2018; Liu et al. 2019c). More importantly, even when data for equivalent nanoparticles are available, there are controversies on the toxic effects found, what derives, in part, from the distinct experimental approaches and lack of standardization of the assay conditions among various laboratories. In the present study, in order to address the impact of surface coating on the NP toxicity profile, we compare, in a single set of experiments, concentration-dependent toxic and behavioral effects of SPIONs synthesized with five different compounds frequently used in biomedical applications: dextran, chitosan, polyethylene glycol, carboxy-silane, and silica. While most of the nanoparticle formulations elicited low levels of toxicity for all end-points tested, chitosan-coated nanoparticles showed the most toxic effects, with mortality levels reaching 100% in the groups treated at concentrations of Fe higher than 2 mM and significant behavioral effects at much lower exposure levels.

## Materials and methods

### Synthesis of the nanoparticles

Iron oxide nanoparticles were synthesized via the polyol route according to a protocol adapted from Forge et al. (2008). Subsequently, the particles were coated, using different procedures, with one of the following compounds: dextran, chitosan, polyethylene glycol, carboxy-silane, and silica. Dextran-coated nanoparticles (SPION-DX) were prepared according to Wunderbaldinger and Oliveira (Wunderbaldinger et al. 2002; Oliveira et al. 2018). Chitosan-coated SPIONs ($M_w$ 90–150 kDa, 75–85% deacetylated) (SPION-CS) were prepared in acetic acid medium, according to the protocol adapted from Mohammadi-Samani et al. (2013). The carboxy-silane coating was performed using 3-(triethoxysilyl) propylsuccinic anhydride (TEPSA) following the procedure of Bridot (Bridot et al. 2013). The resulting shell of carboxy-silane is very thin (~ 1 nm) (SPION-T). For the silica coating, the Stöber process was applied (Stöber 1968), which produced a thicker shell of silica of ~ 12 nm ($SPION@SiO_2$). Polyethylene

glycol-coated NPs (SPION-T-PEG) were prepared adding aminated-PEG ($M_w$ 750 Da) to a batch of SPION-T, following the protocol developed by Stanicki et al. (2014). The final solution of each SPION formulation was purified (according to each protocol) and stored at 4 °C.

Nanoparticle characterization

Fourier transform infrared spectroscopy (FTIR) was used to evaluate the chemical groups present on the NPs. Measurements were performed in a Spectrum One spectrometer (Perkim Elmer) in the spectral range of 4000–400 $cm^{-1}$, with samples in the form of pellets prepared with KBr powder (10% by weight of NPs). The nanoparticle morphology and size distribution were analyzed by transmission electron microscopy (TEM-Tecnai G2 Sphera, from FEI), dripping a small amount of a diluted aliquot on a carbon grid. The hydrodynamic diameter and zeta potential in aqueous solution were measured with a Zetasizer (ZEN3600, Malvern). The crystal structure was obtained from X-ray diffraction measurements (XRD-7000, Shimadzu), using Cu $K_\alpha$ radiation ($\lambda = 1.54$ Å) in steps of 0.05°. The total iron concentration of the NPs was determined either by measuring the longitudinal relaxation rate R1 of the dispersions in a relaxometer (Minispect, Bruker) at a field of 0.47 T and T = 37 °C (Boutry et al. 2009), or by UV-Vis spectroscopy (Wunderbaldinger et al. 2002).

Fish husbandry and embryo collection

Adult wild-type zebrafish animals (*Danio rerio*) of wild-type AB strain were maintained in an automated recirculating system (Tecniplast, Italy) under standard conditions for this species (system water at $28 \pm 2$ °C, pH = 6.5–8.5, and conductivity between 600 and 700 μS) with a 14/10 light/dark photoperiod. Embryos were obtained by crossing females and males at a 1:2 ratio and were separated from unfertilized eggs at 1 hpf (hour post-fertilization) under a stereomicroscope (Nikon, Melville, USA). All experiments were approved by the Institutional Animal Care Committee (CEUA-PUCRS, number 7127) and followed the guidelines of the Brazilian Council of Animal Experimentation for use of fish in research (Concea et al. 2008 and the Brazilian legislation 11.794/08).

Exposure to nanoparticles

Nanoparticles were suspended prior to their use in reverse osmosis filtered water adjusted with commercial salts (*Instant Ocean*®) to meet the species requirements (system water). Animals were exposed to different concentrations (0.125 mM, 0.5 mM, 2.0 mM, and 8.0 mM of SPION-DX, SPION-CS, SPION-T, SPION-T-PEG, and SPION@$SiO_2$ for a total period of 120 h, starting at 1 hpf. An exposure at 0.5 mM corresponds to an iron concentration of 22.3 mg/L in the system water. The medium (water with dispersed NPs) was changed daily until the end of the experiment. Embryos were kept in 24-well cell culture dishes (four embryos per well) in an incubator with controlled photoperiod, temperature, and humidity. A minimum of 32 animals was used per group, in duplicate.

Survival, hatching rates, and anatomical malformations

Animals were evaluated daily for mortality, hatching, and anatomical malformations in the body plane, using a stereomicroscope (Nikon, Melville, USA). The mortality of embryos and larvae was monitored every morning and the dead animals were discarded immediately when detected. The hatching represents the transition point from a developing embryo to a free-living larva and is used to estimate the overall developmental process over time. The hatching rate was accompanied daily until all animals had successfully undergone eclosion. Animals were checked for anatomical malformations every morning until they completed 5 dpf (days post-fertilization), when the incidence of morphological abnormalities in the population was determined. Comparison among groups was based on their dedicated controls.

Exploration of a new environment

The exploratory behavior test was digitally analyzed at 5 dpf in 24-well plates (1 larva per well) with 3 mL of system water. After 1-min acclimation, the exploratory behavior was recorded for 5 min using a HD digital webcam (Quick Cam Pro 9000, Logitech®) as described in detail elsewhere (Creton 2012; Nery et al. 2014). The recorded videos were analyzed using the software EthoVision XT (Noldus®) and the main parameters examined

were the total distance traveled, mean velocity, the time spent in the central and external areas of the well, the percentage of time in a mobile condition, and the number of body rotations greater than 90°. The time spent swimming in the central and external areas of the well is also a parameter used to measure anxiety in zebrafish larvae (Schnörr et al. 2012). These broad exploratory parameters may reflect animals' general physiology and ability to swim and respond to new environmental cues.

### Escape responses

After the exploratory test, animals' cognitive capacity was evaluated by assessing individuals' escape response to an aversive stimulus in consecutive trials ($n = 32$ in duplicates). The larvae were placed on 6-well plates (5 larvae per well) over a LCD monitor in which a red bouncing ball traveled from left to right over a straight 2 cm trajectory covering half of well area (stimuli area), as described in detail by Nery et al. (2014) and adapted from Colwill and Creton (2011) and Creton (2012). The stimuli area was alternated in consecutive 20-s trials to account for spatial and sensory interference. The number of animals that efficiently avoided the stimulus area of the well, escaping to the opposite hemisphere, was counted at the end of each trial.

### Statistical analysis

Survival and hatching rates were analyzed throughout the 5 days of exposure by the long-rank (Mantel-Cox) test. Morphological malformations were evaluated by one-way ANOVA followed by post hoc Tukey test, when significant differences between groups were found. Experimental groups were designed with at least 16 animals each, in duplicate. The significance level was considered $p < 0.05$. Data were analyzed by the GraphPad Prism software and presented as mean values/standard error.

## Results and discussion

### Physicochemical characteristics of the synthesized nanoparticles

Figure 1 summarizes the physicochemical properties of the SPIONs prepared with the different coatings. The

TEM images (Fig. 1a–e) revealed NPs with approximately spherical shape and mean diameters ranging from 6 to 30 nm (Table 1). In most of the cases, this roughly corresponds to the size of the iron oxide core, as the organic coatings are not identifiable in the TEM images. The exception is the SPION@SiO$_2$ particles, where the measured diameter reflects the full size, including the coating. The average diameter of the iron oxide core was comparable in all formulations ranging from 6 to 12 nm. The distribution of hydrodynamic diameters of the nanoparticles in ultrapure water dispersions is shown in Fig. 1f. The mean values, as expected, are larger than the physical sizes measured by TEM (Table 1). We also measured the size distribution of the NPs directly in the zebrafish (system) water. Only minor changes were seen (typically below 20%), as shown in Table 1, indicating that the zebrafish culture medium did not cause further aggregation of the particles. This is important to note as in many studies with SPIONs, the system water provoked substantial increase of the particle's size (Zhu et al. 2012; Ahmad et al. 2015; de Oliveira et al. 2017). During the course of each exposure cycle (24 h), no sign of precipitation was seen on the bottom of the well-plates, indicating that the suspensions kept their state with no significant agglomeration. The zeta potential ($\zeta$) of the different NPs dispersed in ultrapure and system water is also given in Table 1. Most of the nanoparticles showed a reduction in the absolute value of $\zeta$ in zebrafish water as compared to ultrapure dispersions. Nevertheless, this does not affect nanoparticle aggregation, considering that the size distributions were similar in both types of dispersions.

XRD diffractograms (Fig. 1g) confirmed the presence of the crystalline structure of iron oxide in all SPION, except for the SPION@SiO$_2$ where the signal from the relatively thick layer of silica dominates and prevents the detection of the iron oxide core, clearly seen in TEM images (Fig. 1e). The peaks of the inverse spinel cubic structure of magnetite extracted from the reference database (JCPDS-19-629) are also indicated in Fig. 1g. The size of the crystallites calculated using Scherer equation (Cornell and Schwertmann 2003) are displayed in Table 1.

FTIR spectra from the different NPs (Fig. 1h) confirm the chemical structure expected for the different coatings. The absorption band at 587–433 cm$^{-1}$, attributed to Fe-O bonds, and the peak around 3400 cm$^{-1}$, corresponding to the absorption of the hydroxyl group (OH), are present in the spectra of all particles. In the

**Fig. 1** Physicochemical properties of as-prepared SPIONs with different coatings. TEM images of **a** dextran-coated, **b** chitosan-coated, **c** carboxy-silane-coated, **d** PEG-coated, and **e** silica-coated SPIONs (scale bar: 100 nm). **f** Size distribution obtained by DLS of the different NPs dispersed in ultrapure water. **g** FTIR spectra of lyophilized NPs. **h** XDR diffractograms. The dotted lines indicate the peak positions of different planes of the magnetite crystal structure
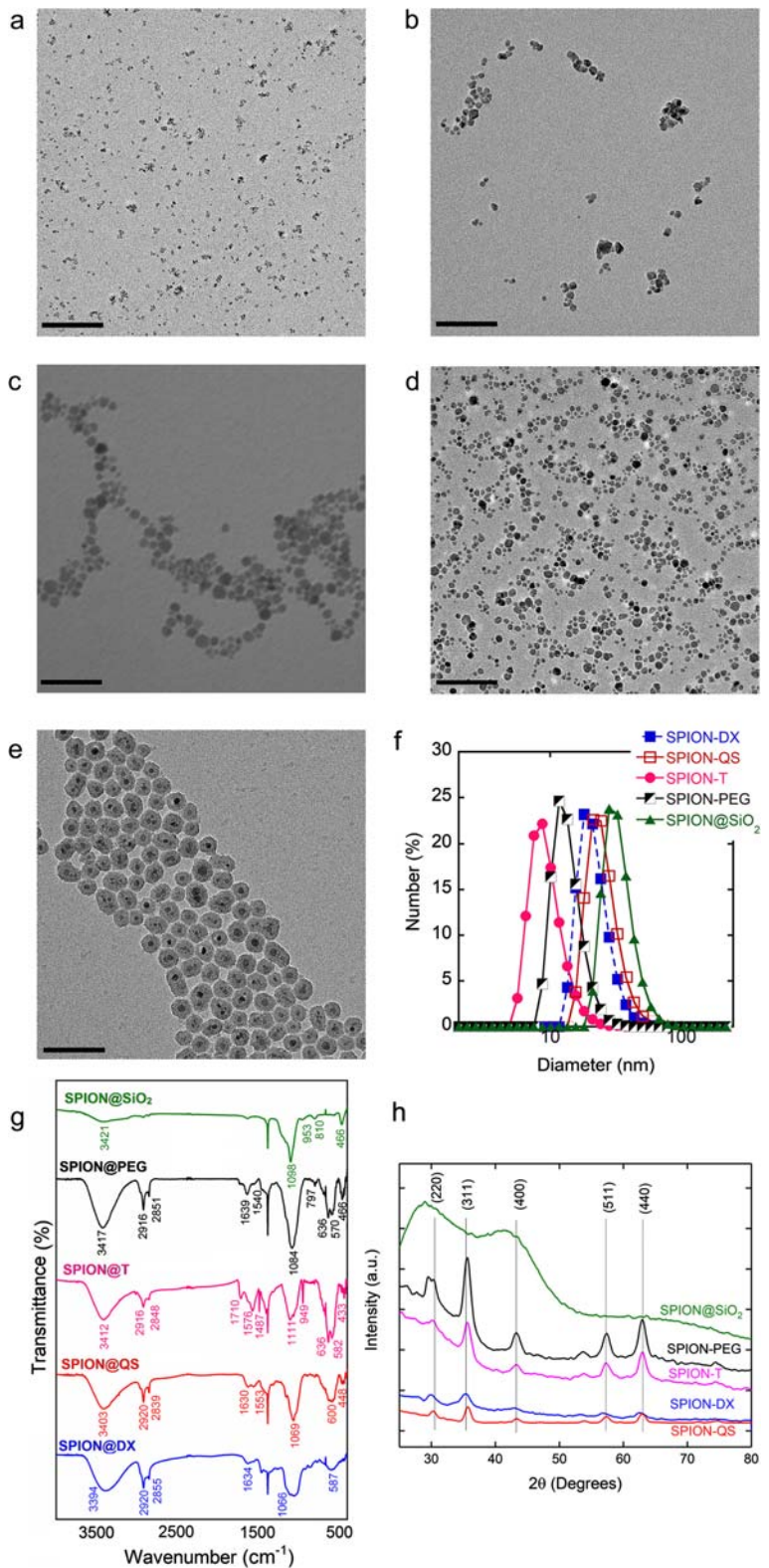
**Table 1** Average physical ($D$) and hydrodynamic ($D_h$) diameters and zeta potential $\zeta$ of the different nanoparticles. TEM data were obtained from direct counting of individual particles. Sizes derived from XRD are obtained from the Scherer equation using the (311) peak. Hydrodynamic diameters and zeta potential were obtained from DLS measurements of nanoparticle dispersions in ultrapure and system water

| Formulation | D (nm) | | $D_h$ (nm) | | $\zeta$ (mV) | |
| --- | --- | --- | --- | --- | --- | --- |
| | TEM | XRD | Ultrapure water | Zebrafish water | Ultrapure water | Zebrafish water |
| SPION-DX | 5.9 ± 1.7 | 5.2 | 22.0 ± 1.4 | 17.2 ± 0.7 | +11.6 ± 0.3 | +4.5 ± 0.30 |
| SPION-CS | 11.7 ± 3.1 | 9.1 | 23.3 ± 3.6 | 28.8 ± 3.4 | +58.7 ± 0.3 | +31.1 ± 0.1 |
| SPION-T | 6.7 ± 2.6 | 6.9 | 10.2 ± 0.9 | 11.4 ± 0.2 | − 37.0 ± 1.5 | − 11.9 ± 2.1 |
| SPION-T-PEG | 9.5 ± 2.5 | 7.4 | 13.8 ± 0.1 | 15.6 ± 0.9 | − 11.5 ± 0.9 | − 7.9 ± 2.4 |
| SPION@SiO$_2$ | 29.5 ± 4.6 | – | 35.9 ± 1.7 | 48.2 ± 4.2 | − 19.5 ± 0.1 | − 18.9 ± 0.5 |

case of SPION@SiO$_2$, the peaks at 953 and 949 cm$^{-1}$ confirm the termination of the silica layer with Si–OH bonds. The peaks at 943 and 797 cm$^{-1}$ are attributed to Si–OH bonds present in the SPION-T and SPION-T-PEG, respectively. Absorption bands of Si–O–Si bonds appear close to 1100 cm$^{-1}$ in the spectra of SPION@SiO$_2$, SPION-T-PEG, and SPION-T. The absorption bands forming two consecutive peaks at around 2919 cm$^{-1}$ and at 2855 cm$^{-1}$ are attributed to the methylene groups (CH$_2$) in the structure of the different organic coatings. The peaks at around 1720 cm$^{-1}$ are attributed to the carbonyl groups (C=O) of in the polysiloxane structures (SPION-T). The peaks at 1069 cm$^{-1}$ are ascribed to the deformation mode of the $\alpha$-glucopyranose ring of the polysaccharides (dextran and chitosan). SPION-DX and SPION-CS spectra show also the presence of amino groups (NH$_2$), around 1640–1630 cm$^{-1}$. The absorption bands at 1540–1553 cm$^{-1}$ are due to amide groups observed in SPION-CS and SPION-T-PEG.

Toxicological effects

The survival rate of zebrafish embryos and larvae exposed to different concentrations of the NPs was determined daily and the results of the Kaplan-Meier test are presented in Fig. 2. Significant changes in mortality rates in relation to the respective control groups were observed only for the exposures with SPION-CS at concentrations of 2.0 and 8.0 mM ($p < 0.0001$) (Fig. 2b). In these cases, the survival rate was dose-dependent and decreased continuously after the second day of exposure. By the end of the fifth day, all embryos from these groups have died. We note that at such concentrations, the SPION-CS precipitated on the well-plates, differently from the other particles in which no visible sign of precipitation was observed. Although the results obtained from colloidal stability of SPION-CS were satisfactory, the temperature ($28 \pm 2$ °C) and pH (7.0–7.5) of the water during the treatments were apparently not favorable to keep the suspension stable.

Anatomical malformations in the larvae from treated and controls groups were also monitored during 5 dpf. The malformations observed included heart edema, reduced swimming bladder, crooked tail, and changes in the yolk aspect or dimensions, as shown in Fig. 3. However, the proportion of animals with malformations in each group (between 3 and 10% at 5 dpf) was at levels naturally expected for the species and was similar between controls and exposed groups, even at the highest concentration of 8.0 mM (Table 2). Average body size was also equivalent among different groups (data not shown). Mortality prevented teratogenicity to be evaluated in groups exposed to SPION-CS at the highest concentrations.

The daily percentage of hatched embryos during the initial 5 dpf are shown in Fig. 4. All embryos from exposed groups and controls hatched between 48 and 72 hpf, as expected for the species (Westerfield 2000), with the exception of animals exposed to chitosan-coated NPs at 8 mM, that died before hatching. Furthermore, slight differences were observed in the hatching dynamics among exposed populations in relation to dedicated control groups. For example, a much larger fraction of eggs exposed to SPION-CS and SPION@SiO$_2$ at 2.0 mM hatched later than in the control group. On the other hand, a slight acceleration of the process was
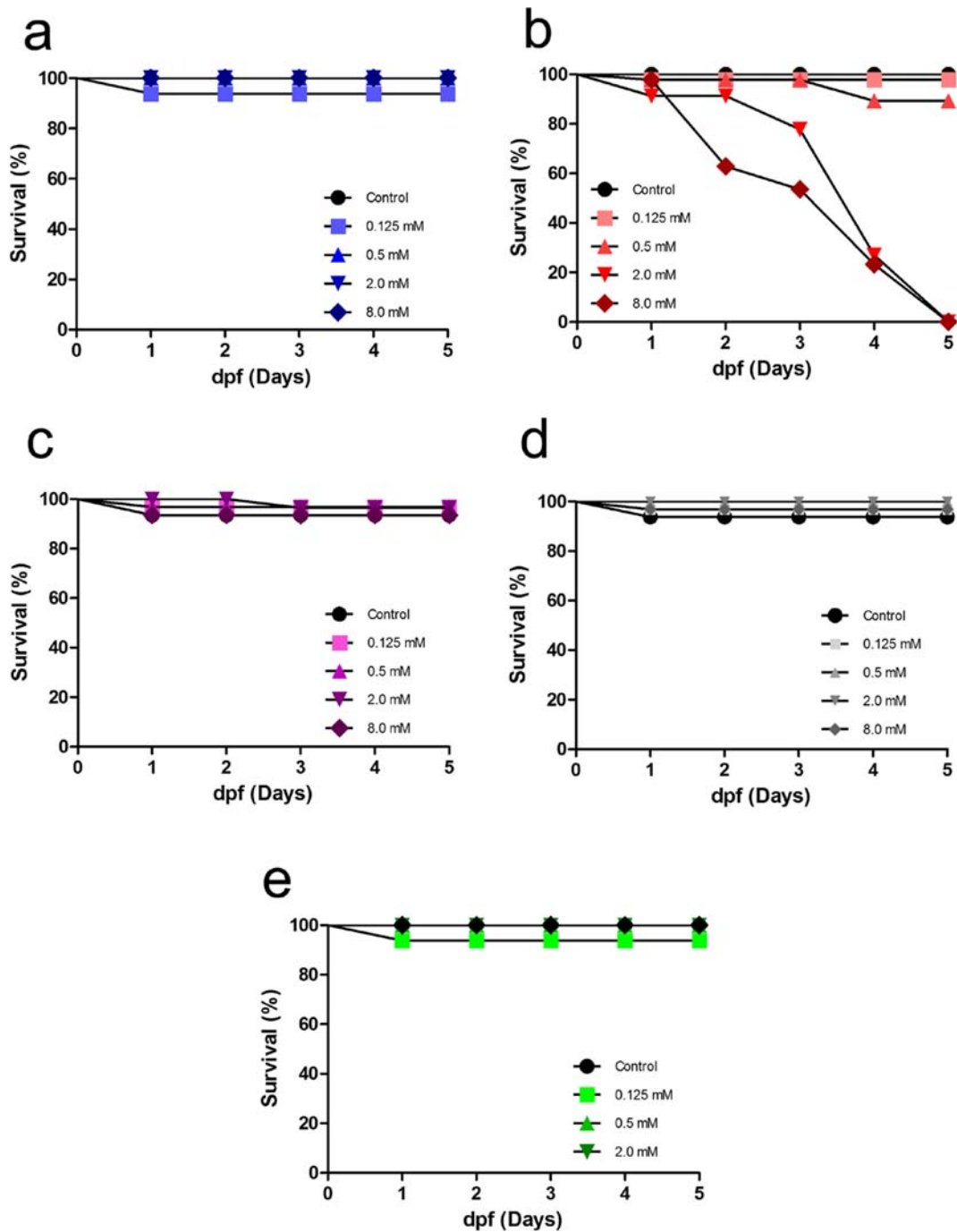
**Fig. 2** Kaplan–Meier survival curves of zebrafish exposed to 0 (controls) and 0.125, 0.5, 2.0, and 8.0 mM of SPIONs, during 5 days of treatment. **a** SPION-DX, **b** SPION-CS, **c** SPION-T, **d** SPION-T-PEG, and **e** SPION@SiO$_2$. Significant differences from the controls were observed for SPION-CS at concentrations of 2.0 and 8.0 mM. Data are expressed as mean ± SE and $n = 32$ animals per group

observed in animals treated with SPION-DX, which was also evident but milder in SPION-T and SPION-T-PEG groups at all concentrations.

Hatching is finely regulated by many endogenous and environmental factors, being sensitive to a variety of chemical agents and medium conditions. Therefore,
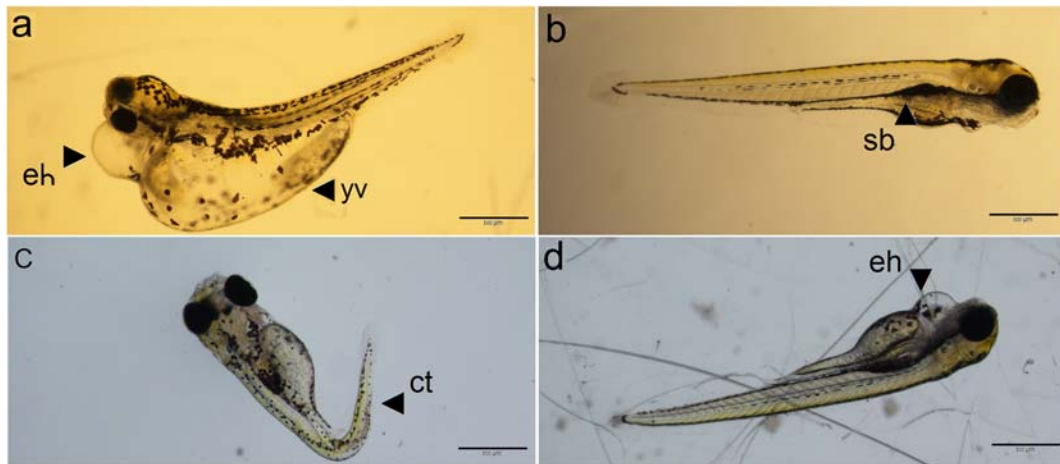
**Fig. 3** Representative images of the most frequent morphological abnormalities observed among individuals from exposed and control groups at 5 dpf. **a** Edema in the heart (eh) and in the yolk sac (ys) in a larva exposed to 0.5 mM SPION-DX. **b** Partially inflated swimming bladder (sb) in a larva exposed to 0.125 mM of SPION-T. **c** Crooked tail (ct) in a larva exposed to 0.5 mM of SPION-T-PEG. **d** Edema in the heart (eh) in a larva exposed to 8.0 mM of SPION-T-PEG. The scale bar size is 500 μm

changes in hatching after nanoparticle exposure have been explored previously to evaluate toxicity in zebrafish (Powers et al. 2010; Asharani et al. 2011; Zhu et al. 2012; Chen et al. 2014; Clemente et al. 2014; Ahmad et al. 2015; Wang et al. 2016; Cambier et al. 2018; Caro et al. 2019). However, the slight changes in the hatching time as seen here cannot be taken as a definitive marker of a deleterious effect. The development process may progress normally, whether or not an embryo has hatched, and the animals that hatch earlier are not significantly underdeveloped than the ones remaining for longer times in their chorions in the short variation range of 1 or 2 days (Westerfield 2000; Zhu et al. 2012).

The toxicological data obtained thus indicate that the differently coated SPIONs were not teratogenic at all exposure levels tested, except in the case of chitosan-coated NPs where 100% mortality at high concentrations, prevented teratogenicity from being assessed. This is in contrast with previous results with uncoated iron oxide NPs where a significant increase in the frequency of malformations was observed in the populations exposed to concentrations larger than 10 mg/L (Zhu et al. 2012). Our results reinforce the general rule that pristine particles are usually more toxic than coated ones due to higher reactivity and poor stability. It is interesting to note that in zebrafish exposed to pure silica NPs at concentrations of 100 or 350 μg/mL, more than 35% of the population developed malformations (Duan et al. 2013; Xue et al. 2013). This is somehow in contradiction with the low levels of teratogenicity of SPION@SiO$_2$ found here, since in both cases, the external surface is chemically similar and silica is the dominant compound.

**Table 2** Incidence of morphological abnormalities (% of affected population) in zebrafish exposed to SPIONs with different coatings

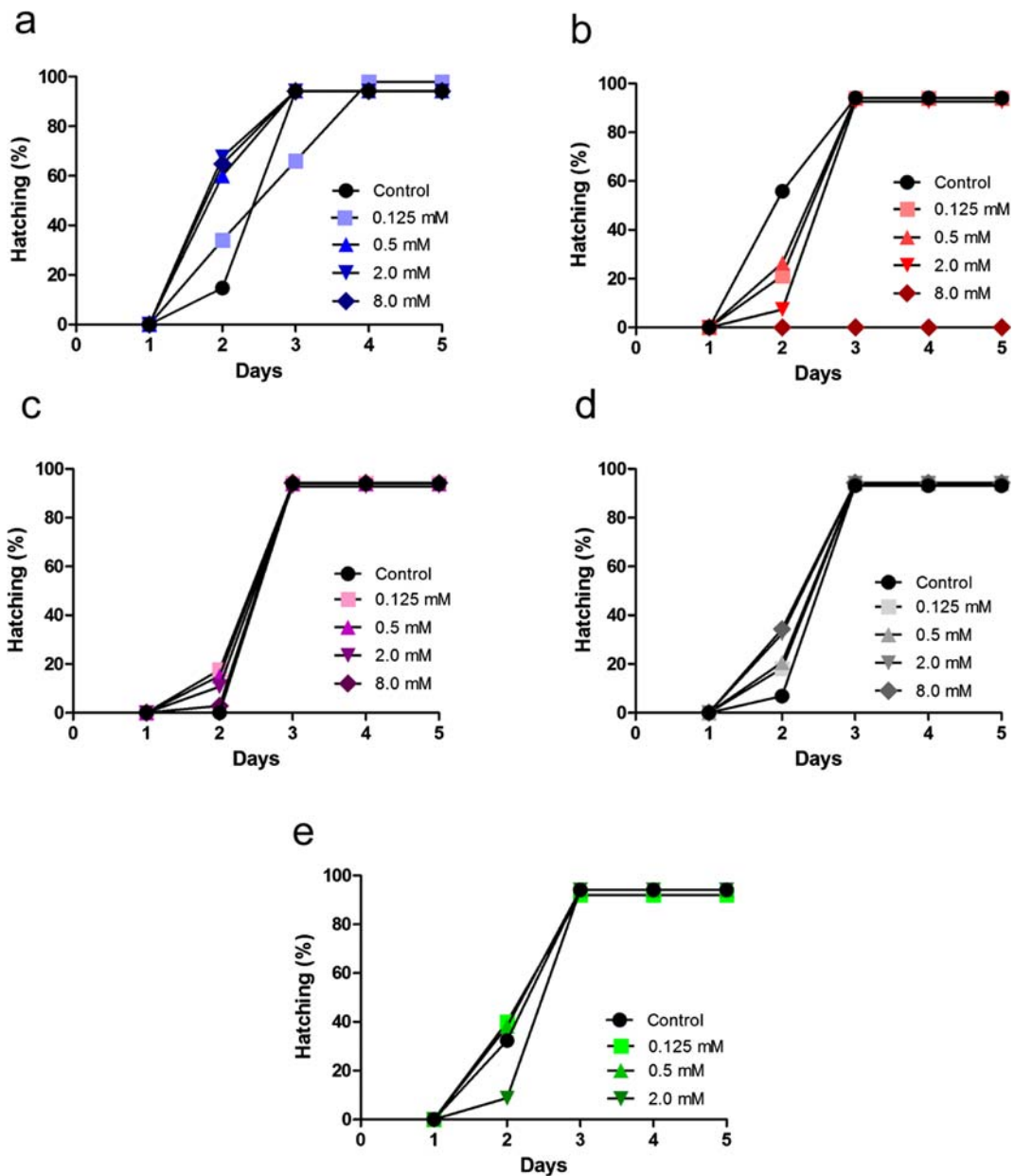| Concentrations (mM) | Malformations (%) | | | | |
|---|---|---|---|---|---|
| | SPION-DX | SPION-CS | SPION-T | SPION-T-PEG | SPION@SiO$_2$ |
| 0[a] | 6.7 | 3.1 | 0 | 6.7 | 9.4 |
| 0.125 | 6.7 | 0 | 3.2 | 0 | 0 |
| 0.5 | 9.4 | 6.9 | 0 | 0 | 0 |
| 2.0 | 3.1 | [b] | 0 | 3.1 | 0 |
| 8.0 | 3.1 | [b] | 0 | 0 | – |

[a] Control groups

[b] 100% of death

Fig. 4 Percentage of hatched embryos after exposure to 0 (controls) and 0.125, 0.5, 2.0, and 8.0 mM of SPIONs during 5 days. **a** SPION-DX ($p = 0.1634$), **b** SPION-CS ($p = 0.0817$), **c** SPION-T ($p = 0.9470$), **d** SPION-T-PEG ($p = 0.8220$), and **e** SPION@SiO$_2$ ($p = 0.6740$), $n = 32$

The increased mortality observed in animals exposed to the higher concentrations of SPION-CS can be associated to poor stability and NP precipitation, as observed in earlier studies with zebrafish embryos using *uncoated* SPIONs (Zhu et al. 2012; de Oliveira et al. 2017). Colloidal instability and precipitation were also evoked to explain toxic effects and increased mortality in zebrafish exposed to other types of uncoated nanoparticles such as ZnO,

CeO$_2$, TiO$_2$, and Ag (Asharani et al. 2011; Kovrižnych et al. 2013; Chen et al. 2014; Ahmad et al. 2015; Wehmas et al. 2015; Lacave et al. 2016; Shih et al. 2016; Xu et al. 2017; Cambier et al. 2018). It has been hypothesized that a large number of NPs adhered on the surface of the chorion may reduce oxygenation in the embryos, leading to death.

Although chitosan is widely regarded as being a non-toxic, biologically compatible polymer, several
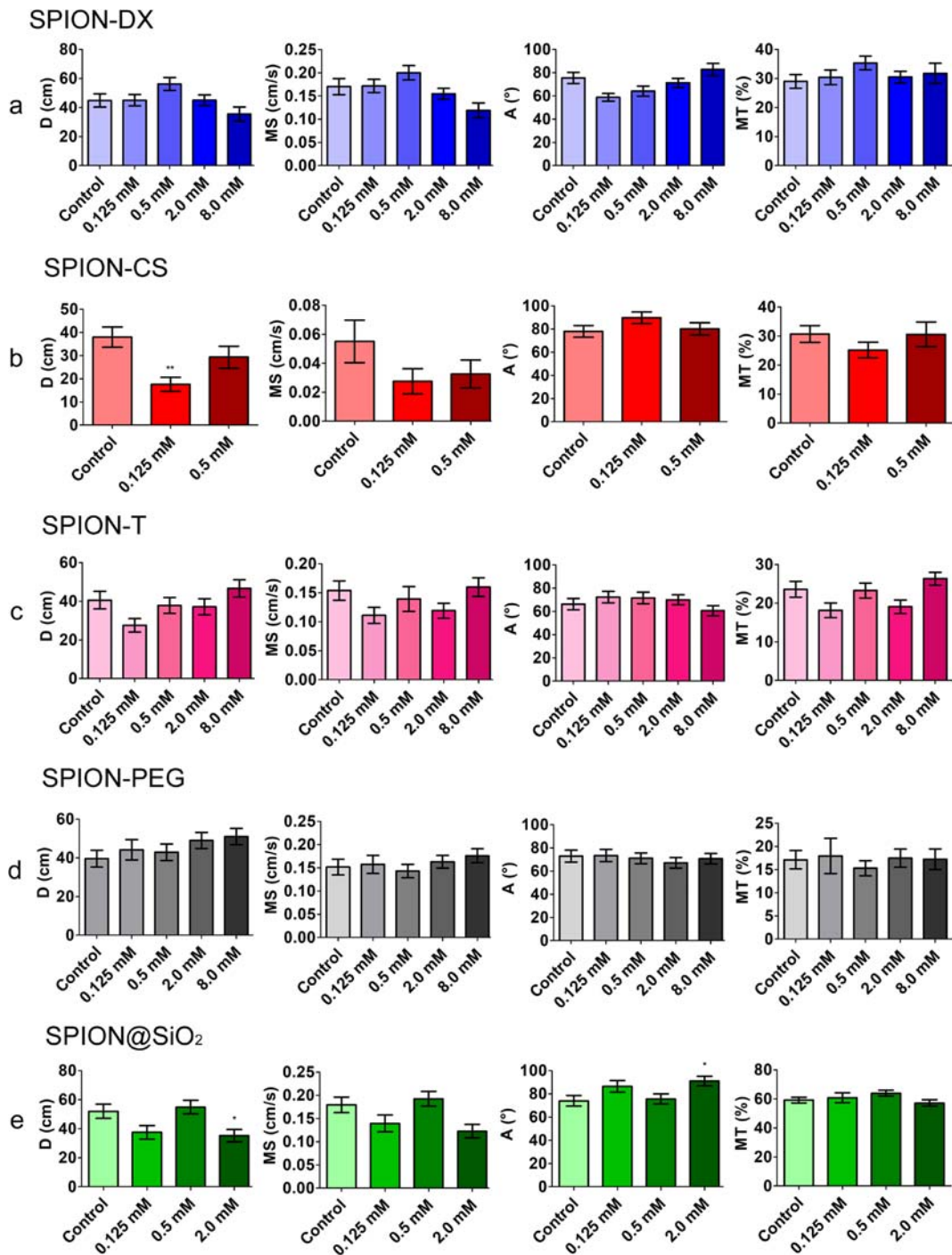
**Fig. 5** Exploratory behavior at 5 dpf after exposure to 0 (controls) and 0.125, 0.5, 2.0, and 8.0 mM of SPIONs, during 5 days. **a** SPION-DX, **b** SPION-QS, **c** SPION-T, **d** SPION-T-PEG, and **e** SPION@SiO₂. Variables are (D) distance traveled, (MS) mean speed, (A) absolute angle of rotation, and (MT) mobile time ($n = 32$; mean ± SE; ANOVA followed by Turkey post hoc; **$p < 0.01$; *$p < 0.05$). Note that data for SPION-CS do not include the higher concentrations due to 100% mortality at 5 dpf

reports challenged this view and raised concerns about its toxicity (see Bellich et al. 2016 for a recent review) especially when administered in the form of nanoparticles. For example, Wang et al.

(2016) compared exposure of zebrafish during 5 dpf to free chitosan and 84-nm diameter chitosan nanoparticles and found hatching delay, increased mortality, and malformations in populations exposed to both formulations in a concentration-dependent profile (Wang et al. 2016). Hu et al. (2011) showed that 200 nm chitosan-NPs at 10–40 μg/mL also caused malformations and an increased rate of cell death, higher levels of reactive oxygen species, and overexpression of heat shock protein 70 (HSP70), indicating that these NPs can cause physiological stress in zebrafish. Our results are coherent with such findings and call for additional mechanistic studies dedicated to chitosan. Microstructural parameters such as the degree of deacetylation and polymerization or the distribution of comonomers along the chains were found to strongly influence chitosan biological activity (Bellich et al. 2016). Investigating such aspects was beyond the scope of the present work, which focused on a general toxicity screening comparing a variety of compounds.

Behavioral analysis

Swimming parameters in larvae are manifestations of behavioral and physiological integrity. Tracking their alteration can be considered an additional and sensitive approach for toxicity evaluation, when compared to the morphological effects or survival. Some of the behavioral parameters evaluated are intrinsically interconnected. The distance traveled, for example, is significantly impacted by the locomotion speed and moving bouts, and this was our motivation to evaluate them simultaneously.

The values of locomotion parameters (distance traveled, mean velocity, absolute turn angle, and percentage of mobile time) in the 5 dpf larvae (exposed and control groups) are shown in Fig. 5. In animals exposed to SPION-DX, SPION-T, and SPION-T-PEG, no significant changes were detected in these parameters in relation to their controls. For the other two coatings, chitosan and silica, a few parameters appeared altered in exposed animals at specific concentrations. Larvae exposed to SPION-CS at 0.125 mM (Fig. 5b) and SPION@SiO$_2$ at 2.0 mM (Fig. 5e) showed a significant decrease in the distance traveled when compared to their dedicated controls ($p = 0.0021$ and $p = 0.004$, respectively). Also, larvae exposed to SPION@SiO$_2$ at 2.0 mM showed a small increase in the turn angle ($p =$

0.0193) (Fig. 5e). These changes are, however, minimal and probably only detectable due to the low variance of the data. Hence, we conclude that under the conditions tested, coated SPIONs did not impact overall locomotor effectiveness or motor accuracy to a significant extent. Previous studies, addressing also other types of nanoparticles such as TiO$_2$, Au, ZnO, and SiO$_2$, found concentration-dependent behavioral changes, including locomotor disturbances in exposed zebrafish larvae (Duan et al. 2013; Xue et al. 2013; Chen et al. 2014; Hu et al. 2017; van Pomeren et al. 2019). Again, in these cases, pristine-uncoated nanoparticles were used.

The time spent in the periphery zone of the well (a parameter related to thigmotaxis) collected for 5 dpf larvae of the different groups is shown in Fig. 6. Again, no significant effect of the exposure to the different particles is observed, suggesting the absence of anxiogenic effects at this developmental stage (Colwill and Creton 2011; Schnörr et al. 2012).

The effect of SPIONs with different coatings on the cognitive ability to escape from a visual aversive stimulus is shown in Fig. 7. Animals exposed to SPION-DX and SPION-T did not show significant differences in the escape response when compared to their controls (Fig. 7a and c). Animals treated with SPION-CS, SPION-T-PEG and SPION@SiO$_2$ showed discrete changes in performance at intermediate concentrations. While SPION-CS at 0.25 and 0.5 mM induced a statistically significant decrease in the escape performance compared to their controls ($p < 0.0001$, Fig. 7b), exposure to SPION-T-PEG at 0.125 mM ($p < 0.0001$), 0.5 mM ($p < 0.0001$), and 2.0 mM ($p < 0.05$), as well as to SPION@SiO$_2$ at 0.125 mM ($p < 0.05$) and 0.5 mM ($p < 0.0001$) resulted in a significant increase in the escape response. The differences observed in the SPION-CS treated groups are more pronounced and may reflect the toxicity of this formulation seen in the previously evaluated parameters. The apparent improvement of performance elicited by the other coatings is modest and may be accounted for by intrinsic variations of behavioral tests combined to effects of group performance cohesion.

Responses motivated by fear are extremely evolutionarily conserved. Cognitively healthy animals tend to escape from the aversive stimulus moving to the opposite area from the one in which the stimulus is presented. The lack of significant effects of the SPIONs on the behavioral exploration and thigmotaxis tests (Figs. 5 and 6) supports the specificity of the observed cognitive effects (Fig. 7), suggesting that they do not arise from
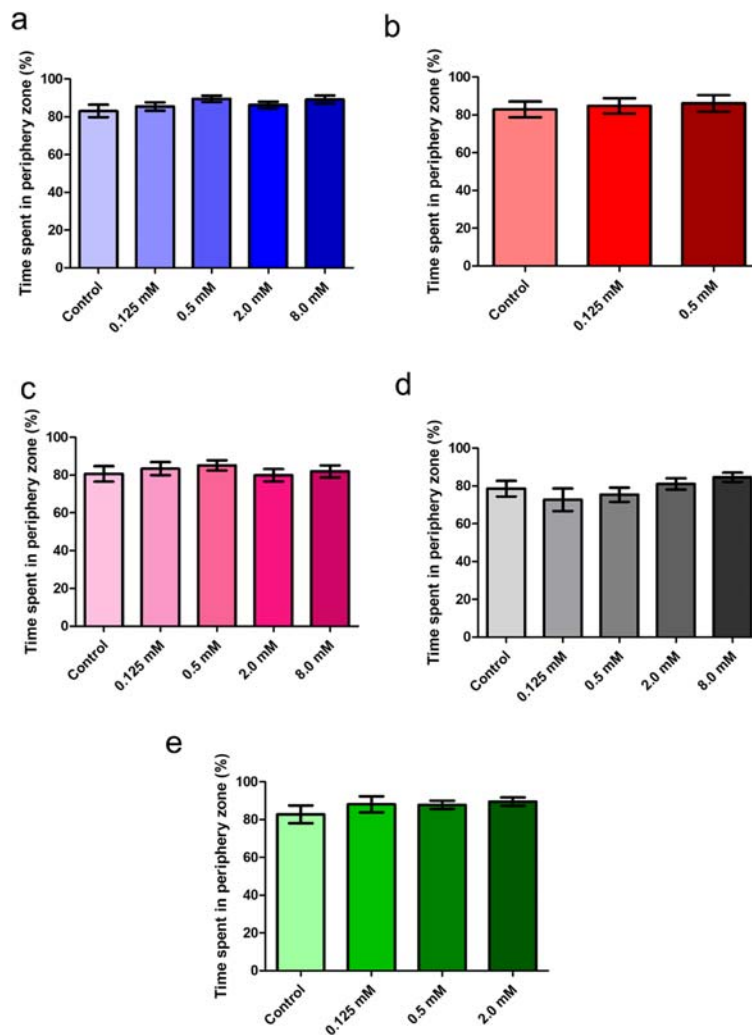
**Fig. 6** Percentage of time spent exploring the periphery zone as a function of NP concentration. The test was acquired after 5-day exposure to SPIONs dispersions at Fe concentrations of 0.125, 0.5, 2.0, and 8.0 mM. **a** SPION-DX, **b** SPION-CS, **c** SPION-T, **d** SPION-T-PEG, and **e** SPION@SiO$_2$ ($n = 32$; mean $\pm$ SE; ANOVA). Note that data for SPION-CS do not include the higher concentrations due to 100% mortality at 5 dpf

altered exploration or motivation deficits. Cognition is complex and multifaceted process that could also be impacted by other physiological mechanisms that were not investigated in our screening. Without further analysis, the underlying cellular and molecular mechanisms of the changes in cognition cannot be attributed to a particular biological system.

## Conclusion

In this work, we evaluated and compared the effect of SPIONS functionalized with five different coatings (dextran, chitosan, polyethylene glycol, carboxysilane, and silica) at various exposure levels on the embryonic development of zebrafish larvae. Our study addresses classical toxicity parameters in zebrafish, including survival, hatching rates, and teratogenicity combined with behavioral and cognitive screenings in a systematic approach to minimize methodological discrepancies that may appear in isolated studies with each type of nanoparticle.

Comparing the different particles, chitosan-coated SPIONs presented the highest toxicity in terms of survival and behavioral parameters, with mortality levels reaching 100% in the groups treated at concentrations of
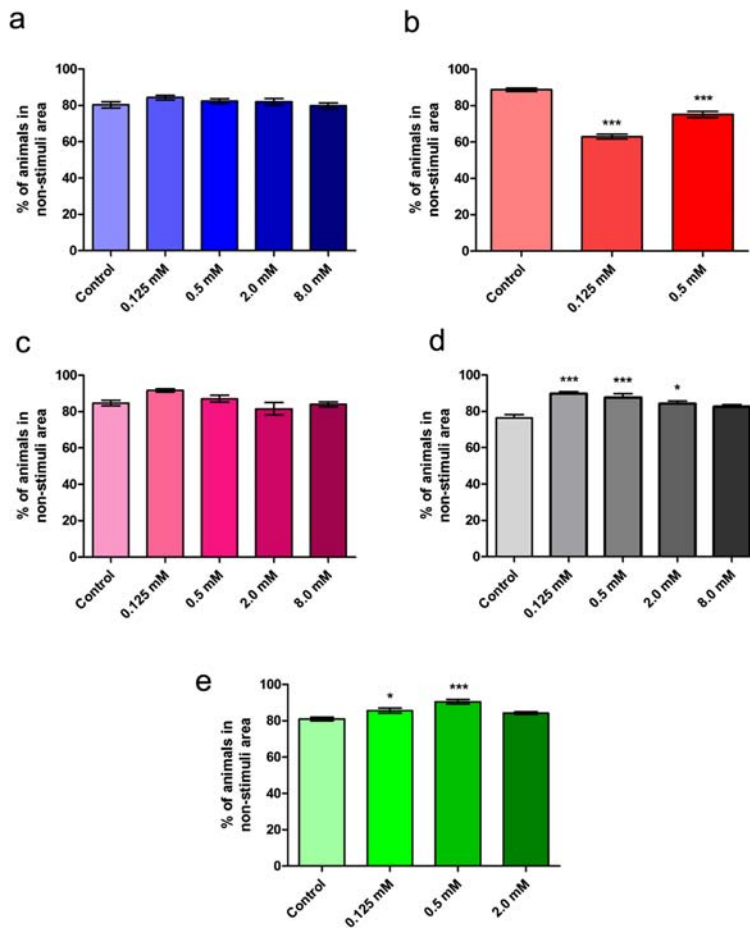
**Fig. 7** Aversive escape behavior responses at 5 dpf after exposure to 0 (controls) and 0.125, 0.5, 2.0, and 8.0 mM of SPIONs during 5 days ($n = 32$; mean ± DP; ANOVA followed by Turkey post hoc, *$p < 0.05$, **$p < 0.01$, ***$p < 0.001$) for **a** SPION-DX, **b** SPION-CS, **c** SPION-T, **d** SPION-T-PEG, and **e** SPION@SiO$_2$. Data for SPION-CS do not include the higher concentrations due to 100% mortality at 5 dpf

Fe higher than 2 mM and significant behavioral and cognitive effects at much lower exposure levels. For he other formulations, toxic effects were in general mild or undetectable for all end-points tested in the investigated concentration range (up to 8 mM of Fe). The incidence of anatomical malformation was low (at baseline levels), contrary to previous observations from exposure to uncoated SPIONS. The exploratory activity and cognitive responses were also not affected significantly, except for some isolated conditions, which deserve further investigation. Taken together, our data show that the coating could affect strongly the toxicity of the nanoparticles, even when the compound is considered biocompatible (as seen in the case of SPION-CS), being a critical parameter in the design of safe nanomaterials.

Here, we performed a broad screening encompassing several nanoparticles and exposure doses that are informative of phenotypic effects and neurobiological and systems integrity. Future studies are needed dedicated to a particular formulation (e.g., SPION-CS), and evaluating other physiological parameters such as hormone levels, neural activity of specific brain areas as well as molecular analysis of the expression of genes related to, e.g., neurotoxicity, inflammation, and apoptosis. We attributed toxicity of SPION-CS mainly to poor colloidal stability. Nevertheless, the role of specific chemical effects associated to chitosan molecular structure was not addressed and deserves further investigation. For that, using (and comparing) chitosans with well-characterized formulations is fundamental, since the large variety of chemical microstructures exhibited by

chitosans has been associated to the conflicting toxicity results found so far for this material.

**Compliance with ethical standards**

All experiments were approved by the Institutional Animal Care Committee (CEUA-PUCRS, number 7127) and followed the guidelines of the Brazilian Council of Animal Experimentation for use of fish in research (Concea et al. 2008) and the Brazilian legislation (11.794/08).

**Conflict of interest**   The authors declare that they have no conflict of interest.

# References

Ahmad F et al (2015) An in vivo evaluation of acute toxicity of cobalt ferrite (CoFe2O4) nanoparticles in larval-embryo Zebrafish (Danio rerio). Aquat Toxicol 166(July):21–28. https://doi.org/10.1016/j.aquatox.2015.07.003

Asharani PV et al (2011) Comparison of the toxicity of silver, gold and platinum nanoparticles in developing zebrafish embryos. Nanotoxicology 5(1):43–54. https://doi.org/10.3109/17435390.2010.489207

Bañobre-López M, Teijeiro A, Rivas J (2013) Magnetic nanoparticle-based hyperthermia for cancer treatment. Rep Pract Oncol Radiother 18(6):397–400. https://doi.org/10.1016/j.rpor.2013.09.011

Bellich B et al (2016) '"The good, the bad and the ugly" of Chitosans'. Marine Drugs 14(5):99. https://doi.org/10.3390/md14050099

Berry CC, Wells S, Charles S, Aitchison G, Curtis AS (2004) Cell response to dextran-derivatised iron oxide nanoparticles post internalisation. Biomaterials 25(23):5405–5413. https://doi.org/10.1016/j.biomaterials.2003.12.046

Biyani N et al (2014) In vitro toxicity assessment of chitosan oligosaccharide coated iron oxide nanoparticles. Toxicol Rep 2:27–39. https://doi.org/10.1016/j.toxrep.2014.11.002

Boutry S et al (2009) How to quantify iron in an aqueous or biological matrix: a technical note. Contrast Media Mol Imaging 4(6):299–304. https://doi.org/10.1002/cmmi.291

Bridot JL, Stanicki D, Laurent S, Boutry S, Gossuin Y, Leclère P, Lazzaroni R, Vander Elst L, Muller RN (2013) New carboxysilane-coated iron oxide nanoparticles for nonspecific cell labelling. Contrast Media Mol Imaging 8(6):466–474. https://doi.org/10.1002/cmmi.1552

Cai W, Chen X (2007) Nanoplatforms for targeted molecular imaging in living subjects. Small 3(11):1840–1854. https://doi.org/10.1002/smll.200700351

Cambier S, Røgeberg M, Georgantzopoulou A, Serchi T, Karlsson C, Verhaegen S, Iversen TG, Guignard C, Kruszewski M, Hoffmann L, Audinot JN, Ropstad E, Gutleb AC (2018) Fate and effects of silver nanoparticles on early life-stage development of zebrafish (Danio rerio) in comparison to silver nitrate. Sci Total Environ 610–611:972–982. https://doi.org/10.1016/j.scitotenv.2017.08.115

Caro C, Egea-Benavente D, Polvillo R, Royo JL, Pernia Leal M, García-Martín ML (2019) Comprehensive toxicity assessment of PEGylated magnetic nanoparticles for in vivo applications. Colloids Surf B: Biointerfaces 177:253–259. https://doi.org/10.1016/j.colsurfb.2019.01.051

Chen TH, Lin CC, Meng PJ (2014) Zinc oxide nanoparticles alter hatching and larval locomotor activity in zebrafish (Danio rerio). J Hazard Mater 277:134–140. https://doi.org/10.1016/j.jhazmat.2013.12.030

Clemente Z, Castro VL, Moura MA, Jonsson CM, Fraceto LF (2014) Toxicity assessment of TiO2 nanoparticles in zebrafish embryos under different exposure conditions. Aquat Toxicol 147:129–139. https://doi.org/10.1016/j.aquatox.2013.12.024

Colwill RM, Creton R (2011) Imaging escape and avoidance behavior in zebrafish larvae. Rev Neurosci 22(1):63–73. https://doi.org/10.1515/RNS.2011.008

Concea, C. N, De C. De E. A. (2008) Peixes mantidos em instalações de instituições de ensino ou pesquisa científica para fins de estudo biológico ou biomédico I, Guia Brasileiro de Produção, Manutenção ou Utilização de Animais para Atividades de Ensino ou Pesquisa Científica. Available at: https://www.mctic.gov.br/mctic/opencms/institucional/concea/paginas/guia.html. Accessed 15 August 2019

Cornell RM, Schwertmann U (2003) The iron oxides. Wiley. https://doi.org/10.1002/3527602097

Creton R (2012) A novel high-throughput imaging system for automated analyses of avoidance behavior in zebrafish larvae. Behav Brain Res 223(1):135–144. https://doi.org/10.1016/j.bbr.2011.04.033

de Oliveira GMT et al (2017) Implications of exposure to dextran-coated and uncoated iron oxide nanoparticles to developmental toxicity in zebrafish. J Nanopart Res 19(12):1–16. https://doi.org/10.1007/s11051-017-4074-5

De Oliveira GMT et al (2014) Transient modulation of acetylcholinesterase activity caused by exposure to dextran-coated iron oxide nanoparticles in brain of adult zebrafish. Comp Biochem Physiol Part - C: Toxicol Pharmacol 162(1):77–84. https://doi.org/10.1016/j.cbpc.2014.03.010

Duan J, Yu Y, Shi H, Tian L, Guo C, Huang P, Zhou X, Peng S, Sun Z (2013) Toxic effects of silica nanoparticles on zebrafish embryos and larvae. PLoS One 8(9):4–12. https://doi.org/10.1371/journal.pone.0074606

Fifi AP et al (2016) Oxytetracycline delivery in adult female zebrafish by iron oxide nanoparticles. Zebrafish 13(6):495–503. https://doi.org/10.1089/zeb.2016.1302

Forge D et al (2008) Optimization of the synthesis of superparamagnetic contrast agents by the design of

experiments method. J Phys Chem C 112(49):19178–19185. https://doi.org/10.1021/jp803832k

Geiss KT et al (2005) In vitro toxicity of nanoparticles in BRL 3A rat liver cells. Toxicol in Vitro 19(7):975–983. https://doi.org/10.1016/j.tiv.2005.06.034

George S, Xia T, Rallo R, Zhao Y, Ji Z, Lin S, Wang X, Zhang H, France B, Schoenfeld D, Damoiseaux R, Liu R, Lin S, Bradley KA, Cohen Y, Nel AE (2011) Use of a high-throughput screening approach coupled with in vivo zebrafish embryo screening to develop hazard ranking for engineered nanomaterials. ACS Nano 5(3):1805–1817. https://doi.org/10.1021/nn102734s

Hill AJ et al (2005) Zebrafish as a model vertebrate for investigating chemical toxicity. Toxicol Sci 86(1):6–19. https://doi.org/10.1093/toxsci/kfi110

Hu Y et al (2011) Toxicity evaluation of biodegradable chitosan nanoparticles using a zebrafish embryo model. Int J Nanomed (6):3351–3359. https://doi.org/10.2147/IJN.S25853

Hu Q et al (2017) 'Effects of titanium dioxide nanoparticles exposure on parkinsonism in zebrafish larvae and PC12. Chemosphere. Elsevier Ltd 173:373–379. https://doi.org/10.1016/j.chemosphere.2017.01.063

Josephson L et al (2002) Near-infrared fluorescent nanoparticles as combined MR/optical imaging probes. Bioconjug Chem 13:554–560. https://doi.org/10.1021/bc015555d

Kari G, Rodeck U, Dicker AP (2007) Zebrafish: an emerging model system for human disease and drug discovery. Clin Pharmacol Ther 82(1):70–80. https://doi.org/10.1038/sj.clpt.6100223

Karunaratne DP et al (2017) Developmental toxicity of glycine-coated silica nanoparticles in embryonic zebrafish. Environ Pollut 229:439–447. https://doi.org/10.1016/j.envpol.2017.06.016

Kong B, Seog JH, Graham LM, Lee SB (2011) Experimental considerations on the cytotoxicity of nanoparticles. Nanomedicine 6(5):929–941. https://doi.org/10.2217/nnm.11.77

Koo OM, Rubinstein I, Onyuksel H (2005) Role of nanotechnology in targeted drug delivery and imaging: a concise review. Nanomedicine 1(3):193–212. https://doi.org/10.1016/j.nano.2005.06.004

Kovrižnych JA, Sotníková R, Zeljenková D, Rollerová E, Szabová E, Wimmerová S (2013) Acute toxicity of 31 different nanoparticles to zebrafish (Danio rerio) tested in adulthood and in early life stages - comparative study. Interdiscip Toxicol 6(2):67–73. https://doi.org/10.2478/intox-2013-0012

Lacave JM et al (2016) Effects of metal-bearing nanoparticles (Ag, Au, CdS, ZnO, SiO2) on developing zebrafish embryos. Nanotechnology 27(32):1–15. https://doi.org/10.1088/0957-4484/27/32/325102

Laurent S, Forge D, Port M, Roch A, Robic C, Vander Elst L, Muller RN (2008) Magnetic iron oxide nanoparticles: synthesis, stabilization, vectorization, physicochemical characterizations and biological applications. Chem Rev 108(6):2064–2110. https://doi.org/10.1021/cr068445e

Lee N, Yoo D, Ling D, Cho MH, Hyeon T, Cheon J (2015) Iron oxide based nanoparticles for multimodal imaging and magnetoresponsive therapy. Chem Rev 115(19):10637–10689. https://doi.org/10.1021/acs.chemrev.5b00112

Lieschke GJ, Currie PD (2007) Animal models of human disease: zebrafish swim into view. Nat Rev Genet 8(5):353–367. https://doi.org/10.1038/nrg2091

Lin S, Zhao Y, Nel AE, Lin S (2013) Zebrafish: an in vivo model for Nano EHS studies. Small 9(9–10):1608–1618. https://doi.org/10.1002/smll.201202115

Liskova A et al (2017) Immunotoxicity, genotoxicity and epigenetic toxicity of nanomaterials: new strategies for toxicity testing? Food Chem Toxicol 109:797–811. https://doi.org/10.1016/j.fct.2017.08.030

Liu H, Wang X, Wu Y, Hou J, Zhang S, Zhou N, Wang X (2019a) Toxicity responses of different organs of zebrafish (Danio rerio) to silver nanoparticles with different particle sizes and surface coatings. Environ Pollut 246:414–422. https://doi.org/10.1016/j.envpol.2018.12.034

Liu R et al (2012) Automated phenotype recognition for zebrafish embryo based in vivo high throughput toxicity screening of engineered nano-materials. PLoS One 7(4):e35014. https://doi.org/10.1371/journal.pone.0035014

Liu X, Peng M, Li G, Miao Y, Luo H, Jing G, He Y, Zhang C, Zhang F, Fan H (2019b) Ultrasonication-triggered ubiquitous assembly of magnetic janus amphiphilic nanoparticles in cancer theranostic applications. Nano Lett 19(6):4118–4125. https://doi.org/10.1021/acs.nanolett.9b01524

Liu X, Peng M, Li G, Miao Y, Luo H, Jing G, He Y (2019c) 'Ultrasonication-triggered ubiquitous assembly of magnetic janus amphiphilic nanoparticles in cancer theranostic applications. Nano Lett Am Chem Soc 19:4118–4125. https://doi.org/10.1021/acs.nanolett.9b01524

Magro M, de Liguoro M, Franzago E, Baratella D, Vianello F (2018) The surface reactivity of iron oxide nanoparticles as a potential hazard for aquatic environments: a study on Daphnia magna adults and embryos. Sci Rep 8(1):1–15. https://doi.org/10.1038/s41598-018-31483-6

Mahmoudi M, Sant S, Wang B, Laurent S, Sen T (2011) Superparamagnetic iron oxide nanoparticles (SPIONs): development, surface modification and applications in chemotherapy. Adv Drug Deliv Rev 63(1–2):24–46. https://doi.org/10.1016/j.addr.2010.05.006

Mohammadi-Samani S et al (2013) Preparation and assessment of chitosan-coated superparamagnetic Fe3O4 nanoparticles for controlled delivery of methotrexate. Res Pharm Sci 8(1):25–33

Montet X, Weissleder R, Josephson L (2006) Imaging pancreatic cancer with a peptide-nanoparticle conjugate targeted to normal pancreas. Bioconjug Chem 17(4):905–911. https://doi.org/10.1021/bc060035+

Nery LR et al (2014) 'Brain intraventricular injection of amyloid-β in zebrafish embryo impairs cognition and increases tau phosphorylation, effects reversed by lithium. PLoS One 9(9):e105862. https://doi.org/10.1371/journal.pone.0105862

Oliveira E et al (2018) Synthesis and nuclear magnetic relaxation properties of composite iron oxide nanoparticles. Química Nova 42(1):57–64. https://doi.org/10.21577/0100-4042.20170309

Osborne OJ, Johnston BD, Moger J, Balousha M, Lead JR, Kudoh T, Tyler CR (2013) Effects of particle size and coating on nanoscale Ag and TiO 2 exposure in zebrafish (Danio rerio) embryos. Nanotoxicology 7(8):1315–1324. https://doi.org/10.3109/17435390.2012.737484

Powers CM et al (2010) Silver exposure in developing zebrafish (Danio rerio): persistent effects on larval behavior and survival. Neurotoxicol Teratol 32(3):391–397. https://doi.org/10.1016/j.ntt.2010.01.009

Powers CM, Slotkin TA, Seidler FJ, Badireddy AR, Padilla S (2011) Silver nanoparticles alter zebrafish development and larval behavior: distinct roles for particle size, coating and composition. Neurotoxicol Teratol 33(6):708–714. https://doi.org/10.1016/j.ntt.2011.02.002

Ramos AP, Cruz MAE, Tovani CB, Ciancaglini P (2017) Biomedical applications of nanotechnology. Biophys Rev 9(2):79–89. https://doi.org/10.1007/s12551-016-0246-2

Reimer P et al (2007) SPIO-enhanced 2D-TOF MR angiography of the portal venous system: results of an intraindividual comparison. J Magn Reson Imaging 7(6):945–949. https://doi.org/10.1002/jmri.1880070602

Samaee SM, Rabbani S, Jovanović B, Mohajeri-Tehrani MR, Haghpanah V (2015) Efficacy of the hatching event in assessing the embryo toxicity of the nano-sized TiO2 particles in zebrafish: a comparison between two different classes of hatching-derived variables. Ecotoxicol Environ Saf 116: 121–128. https://doi.org/10.1016/j.ecoenv.2015.03.012

Schnörr SJ, Steenbergen PJ, Richardson MK, Champagne DL (2012) Measuring thigmotaxis in larval zebrafish. Behav Brain Res 228(2):367–374. https://doi.org/10.1016/j.bbr.2011.12.016

Sharifi S, Seyednejad H, Laurent S, Atyabi F, Saei AA, Mahmoudi M (2015) Superparamagnetic iron oxide nanoparticles for in vivo molecular and cellular imaging. Contrast Media Mol Imaging 10(5):329–355. https://doi.org/10.1002/cmmi.1638

Shih YJ, Su CC, Chen CW, Dong CD, Liu WS, Huang CP (2016) Adsorption characteristics of nano-TiO2 onto zebrafish embryos and its impacts on egg hatching. Chemosphere 154:109–117. https://doi.org/10.1016/j.chemosphere.2016.03.061

Soenen SJH et al (2011) Cytotoxic effects of iron oxide nanoparticles and implications for safety in cell labelling. Biomaterials 32(1):195–205. https://doi.org/10.1016/j.biomaterials.2010.08.075

Som C, Wick P, Krug H, Nowack B (2011) Environmental and health effects of nanomaterials in nanotextiles and façade coatings. Environ Int 37(6):1131–1142. https://doi.org/10.1016/j.envint.2011.02.013

Stanicki D et al (2014) Carboxy-silane coated iron oxide nanoparticles: a convenient platform for cellular and small animal imaging. J Mater Chem B 2(4):387–397. https://doi.org/10.1039/c3tb21480j

Sun Z et al (2013) Characterization of cellular uptake and toxicity of aminosilane-coated iron oxide nanoparticles with different charges in central nervous system-relevant cell culture models. Int J Nanomedicine 8:961–970. https://doi.org/10.2147/IJN.S39048

Stöber AF (1968) Facial feature extraction using improved deformable templates. J Colloid Interface Sci 26:62–69. https://doi.org/10.1109/ICOSP.2006.345929

van der Merwe D and Pickrell JA (2007) 'Toxicity of nanomaterials', in Veterinary Toxicology. Elsevier, pp 319–326. https://doi.org/10.1016/B978-0-12-370467-2.X5095-0

van Pomeren M et al (2019) The biodistribution and immunoresponses of differently shaped non-modified gold particles in zebrafish embryos. Nanotoxicology 13(4):558–571. https://doi.org/10.1080/17435390.2018.1564079

Vu AT et al (2004) First-pass contrast-enhanced magnetic resonance angiography in humans using ferumoxytol, a novel ultrasmall superparamagnetic iron oxide (USPIO)-based blood pool agent. J Magn Reson Imaging 21(1):46–52. https://doi.org/10.1002/jmri.20235

Wang Y et al (2016) Characterization and toxicology evaluation of chitosan nanoparticles on the embryonic development of zebrafish, Danio rerio. Carbohydr Polym 141(1):204–210. https://doi.org/10.1016/j.carbpol.2016.01.012

Wang Y-XJ (2015) Current status of superparamagnetic iron oxide contrast agents for liver magnetic resonance imaging. World J Gastroenterol 21(47):13400. https://doi.org/10.3748/wjg.v21.i47.13400

Wehmas LC, Anders C, Chess J, Punnoose A, Pereira CB, Greenwood JA, Tanguay RL (2015) Comparative metal oxide nanoparticle toxicity using embryonic zebrafish. Toxicol Rep 2:702–715. https://doi.org/10.1016/j.toxrep.2015.03.015

Westerfield M (2000) The zebrafish book. A guide for the laboratory use of zebrafish (Danio rerio). Eugene: University of Oregon Press. Available at: http://zfin.org/zf_info/zfbook/zfbk.html. Accessed 20 August 2001

Wunderbaldinger P, Josephson L, Weissleder R (2002) Crosslinked iron oxides (CLIO): A new platform for the development of targeted MR contrast agents. Acad Radiol 9:304–306. https://doi.org/10.1016/S1076-6332(03)80210-6

Xu J, Zhang Q, Li X, Zhan S, Wang L, Chen D (2017) The effects of copper oxide nanoparticles on dorsoventral patterning, convergent extension, and neural and cardiac development of zebrafish. Aquat Toxicol 188:130–137. https://doi.org/10.1016/j.aquatox.2017.05.002

Xue JY et al (2013) An assessment of the impact of SiO2 nanoparticles of different sizes on the rest/wake behavior and the developmental profile of zebrafish larvae. Small 9(18):3161–3168. https://doi.org/10.1002/smll.201300430

Xue W, Liu Y, Zhang N, Yao Y, Ma P, Wen H, Huang S, Luo Y, Fan J (2018) Effects of core size and PEG coating layer of iron oxide nanoparticles on the distribution and metabolism in mice. Int J Nanomedicine 13:5719–5731. https://doi.org/10.2147/IJN.S165451

Zhang H, Li L, Liu XL, Jiao J, Ng CT, Yi JB, Luo YE, Bay BH, Zhao LY, Peng ML, Gu N, Fan HM (2017) Ultrasmall ferrite nanoparticles synthesized via dynamic simultaneous thermal decomposition for high-performance and multifunctional T1 magnetic resonance imaging contrast agent. ACS Nano 11(4):3614–3631. https://doi.org/10.1021/acsnano.6b07684

Zhu X, Tian S, Cai Z (2012) Toxicity assessment of iron oxide nanoparticles in zebrafish (Danio rerio) early life stages. PLoS One 7(9):1–6. https://doi.org/10.1371/journal.pone.0046286